Non-Hermitian skin effect in magnetic systems

Kuangyin Deng [*] and Benedetta Flebus[†]

Department of Physics, Boston College, 140 Commonwealth Avenue, Chestnut Hill, Massachusetts 02467, USA

Far from being limited to a trivial generalization of their Hermitian counterparts, non-Hermitian topological phases have gained widespread interest due to their unique properties. One of the most striking non-Hermitian phenomena is the skin effect, i.e., the localization of a macroscopic fraction of bulk eigenstates at a boundary, which underlies the breakdown of the bulk-edge correspondence. Here we develop a generic phenomenological approach to describing magnetic dissipation within a lattice model and we introduce an "effective area law" to investigate the emergence of the skin effect in magnetic systems. As a testbed of our approach, we focus on a spin-orbit-coupled van der Waals (vdW) ferromagnet with spin-nonconserving magnon-phonon interactions, finding that the magnetic skin effect emerges in an appropriate temperature regime. Our results suggest that the interference between Dzyaloshinskii-Moriya interaction (DMI) and nonlocal magnetic dissipation plays a key role in the accumulation of bulk states at the boundaries.

Introduction For decades the application of topology in condensed matter has relied on the principle of the bulk-edge correspondence, according to which the edge states of a system, which appear under open boundary conditions, can be characterized by a topological invariant calculated on a Brillouin zone defined under periodic boundary conditions [1]. In some non-Hermitian systems, however, this fundamental correspondence has been found to be broken [2–15]. As a result, bulk modes can no longer be described by Bloch's theorem as delocalized plane waves. Instead, a macroscopic number of bulk states localize at a boundary of the system, i.e., a phenomenon dubbed as the non-Hermitian skin effect.

The skin effect has been extensively investigated in one-dimensional (1d) asymmetric Su-Schrieffer-Heeger (SSH) models [4,7,16–20], in which the pile-up of bulk modes at one system's edge can be understood in terms of the imbalance hopping in the left and right directions. Experimentally, the skin effect has been uncovered in photonic systems and metamaterials with judiciously engineered non-Hermitian interactions, while its observation in a naturally occurring solid-state system has not yet been reported [17,21–24].

Magnons, i.e., the collective excitations of magnetic systems, are bosonic quasiparticles whose number is not conserved and whose dynamics is intrinsically non-Hermitian [25–30]. Their fundamental properties, including their lifetime, can be easily tuned via external fields and drives, making them promising solid-state candidates for the exploration of non-Hermitian topological phenomena [31–34]. In this Letter, we investigate the emergence of the skin effect in insulating two-dimensional (2d) magnetic systems, in which non-Hermitian terms that violate the bulk-edge correspondence arise from intrinsic spin nonconserving interactions.

The physics of dissipative interactions in magnetic systems are very complex and the effective magnon lifetime stems from a variety of spin-wave decay mechanisms, e.g., magnon-magnon, magnon-electron, and magnon-phonon interactions, and magnon scattering on extrinsic impurities. Several theoretical papers have addressed [35–42] the dissipation due to one of the aforementioned mechanisms and have provided approximate expressions for the magnon relaxation time. These expressions are, however, often given in the continuum limit and can not be readily incorporated in a lattice model, which is an essential starting point for the investigation of the skin effect. Since a comprehensive microscopic description of the magnetic dissipative dynamics within a lattice model is a particularly challenging (and yet untackled) task, here we propose a generic phenomenological approach that can be tested against *ab initio* or experimental data. Our approach serves as a general recipe of constructing an effective non-Hermitian Hamiltonian from bands broadening data. Inspired by the area law proposed by Ref. [43], here we introduce an "effective area law" that is complimentary to our phenomenological approach to magnetic dissipation and can serve as a criteria for the emergence of the skin effect in any 2d magnetic system.

As a concrete example of our approach, we focus on a ferromagnetic spin-orbit-coupled insulating vdW monolayer. Recent *ab initio* studies have addressed the phonon-driven dissipation of the eigenmodes of a vdW magnetic system and calculated its behavior over a large portion of the first Brillouin zone [44]. Here, we develop a phenomenological model for the dissipative terms that is consistent with the aforementioned *ab initio* results, while respecting the symmetries of the honeycomb lattice. We find that, away from the long-wavelength limit (but below the magnetic ordering temperature), the magnetic skin effect appears, i.e., a macroscopic number of the bulk spin-wave modes accumulate at the armchair terminations of a nanoribbon. Our results show that the localization of the bulk states relies on the interference

---

[*]dengku@bc.edu
[†]flebus@bc.edu

between the Dzyaloshinskii-Moriya interactions and nonlocal dissipative terms.

Hermitian spin model. We consider a vdW ferromagnetic monolayer whose Hermitian spin dynamics is described by the Hamiltonian

$$\mathcal{H} = -J \sum_{\langle i,j \rangle} \mathbf{S}_i \cdot \mathbf{S}_j - J_2 \sum_{\langle\langle i,j \rangle\rangle} \mathbf{S}_i \cdot \mathbf{S}_j$$
$$- B \sum_i S_i^z + D \sum_{\langle\langle i,j \rangle\rangle} v_{ij} \hat{\mathbf{z}} \cdot (\mathbf{S}_i \times \mathbf{S}_j), \quad (1)$$

where $J > 0$ is the nearest-neighbor (NN) Heisenberg exchange, $J_2 > 0$ the next-to-nearest-neighbor (NNN) exchange coupling, $B \geqslant 0$ the out-of-plane magnetic field, D the NNN DMI strength, and $v_{ij} = -v_{ji} = \pm 1$ reflects the nonreciprocity of the DM interactions. Far below the magnetic ordering temperature T_c, i.e., for $T \ll T_c$, and for $D \leqslant (J + 4J_2)/\sqrt{3}$, we can access the magnon spectrum by introducing the linearized Holstein-Primakoff transformation with respect to an uniform ground state, i.e.,

$$S_i^+ = S_i^x + i S_i^y \approx \sqrt{2S} d_i, \quad S_i^z = S - d_i^\dagger d_i, \quad (2)$$

where S is the classical spin (in units of $\hbar$) and d_i ($d_i^\dagger$) the magnon annihilation (creation) operator at the ith site, which obeys the bosonic commutation relation $[d_i, d_j^\dagger] = \delta_{ij}$. Plugging Eq. (2) into Eq. (1) and truncating the Hamiltonian beyond quadratic terms in the Holstein-Primakoff bosons, we find

$$\mathcal{H} = (3JS + 6J_2 S + B) \sum_i d_i^\dagger d_i - JS \sum_{\langle i,j \rangle} (d_i^\dagger d_j + \text{H.c.})$$
$$- J_2 S \sum_{\langle\langle i,j \rangle\rangle} (d_i^\dagger d_j + \text{H.c.}) - DS \sum_{\langle\langle i,j \rangle\rangle} (i v_{ij} d_i^\dagger d_j + \text{H.c.}). \quad (3)$$

Performing a Fourier transformation while introducing the spinor $\Psi_k = (a_k, b_k)$, where a_k (b_k) is the Fourier transform of the magnon annihilation operator on the A (B) sublattice, Eq. (3) becomes

$$\mathcal{H} = \sum_{i=0,x,y,z} \sum_k \Psi_k^\dagger (h_i \sigma_i) \Psi_k, \quad (4)$$

with

$$h_0 = 3JS + 6J_2 S + B - 4J_2 S \sum_n \cos k \cdot \boldsymbol{\beta}_n,$$

$$h_x = -JS \sum_n \cos k \cdot \boldsymbol{\alpha}_n,$$

$$h_y = JS \sum_n \sin k \cdot \boldsymbol{\alpha}_n, \quad h_z = 2DS \sum_n \sin k \cdot \boldsymbol{\beta}_n, \quad (5)$$

where the $\boldsymbol{\alpha}_n$ and $\boldsymbol{\beta}_n$ (with $n = 1, 2, 3$) are, respectively, the NN and NNN bond vectors depicted in Fig. 1(a). Here and in what follows, we omit the explicit dependence of the function h_i (for $i = x, y, z$) on the wavevector k.

Non-Hermitian dissipative terms. The magnon number is not conserved due to ubiquitous spin nonconserving interactions of magnons with the crystalline lattice [35–41]. Several *ab initio* studies have investigated the dissipation of magnetic eigenmodes driven by magnon-phonon interactions,
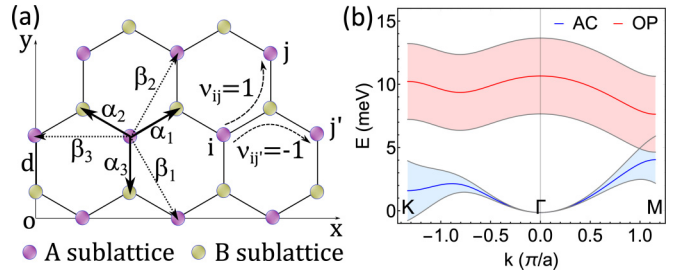

FIG. 1. (a) Ferromagnetic honeycomb lattice. $\boldsymbol{\alpha}_n$ and $\boldsymbol{\beta}_n$ are the NN and NNN bond vectors, respectively. $v_{ij} = 1$ and $v_{ij'} = -1$ label the sign of counterclockwise and clockwise DMI, respectively. (b) Spin-wave dispersions with broadening along a representative path ($\Gamma - K - M$) in the first Brillouin zone. The blue and red lines indicate the real spectra of the acoustic (AC) and optical (OP) mode, respectively. The light-blue and light-red shadows represent the band broadenings ΔE_{ac} and ΔE_{opt}, respectively. Here $a = \sqrt{3}d$ is the distance between A-A (B-B) sublattices, where d is the NN A-B distance.

modeled via finite-temperature random phonon fluctuations that modify the distance between neighboring spins [44–46]. The linewidth broadening of the acoustic ΔE_{ac} and optical ΔE_{op} eigenmodes of a magnetic honeycomb lattice have been found to scale, respectively, as $\Delta E_{ac} \propto k^2$ (with $k = |\mathbf{k}|$) and $\Delta E_{op} \propto constant$ over a large portion of the first Brillouin zone [44]. While the broadening of the optical eigenmode is a constant that can be readily incorporated in the lattice Hamiltonian, we cannot include the relaxation associated with the acoustic mode in the present form $\propto k^2$ as it explicitly breaks the translational symmetry of our model [47].

In order to construct an effective non-Hermitian Hamiltonian that reproduces the observed band broadening, here we adopt a phenomenological approach, i.e., we include non-Hermitian terms allowed by symmetry. Specifically, we use a Fourier series (i.e., a complete basis) to describe a generic non-Hermitian contribution ΔE to the energy, i.e., $\Delta E = -i \sum_{l=0}^{\infty} [\sum_{n_1} (\zeta_{l\alpha}^1 \cos lk \cdot \boldsymbol{\alpha}_{n_1} + \zeta_{l\alpha}^2 \sin lk \cdot \boldsymbol{\alpha}_{n_1}) + \sum_{n_2} (\zeta_{l\beta}^1 \cos lk \cdot \boldsymbol{\beta}_{n_2} + \zeta_{l\beta}^2 \sin lk \cdot \boldsymbol{\beta}_{n_2}) + ...]$, where "..." represents longer crystalline vectors in higher orders. Here $n_1 (n_2)$ is the number of the crystalline vectors of the nearest (next-to-nearest) neighbors and $\zeta^{1(2)}$ is the phenomenological coefficient of each term for cosine (sine) functions in unit of energy. For purely dissipative processes, i.e., in the absence of gain, we require $\text{Im}(\Delta E) \leqslant 0$. For consistency, we retain terms of the same order in reciprocal vectors as the Hermitian Hamiltonian. Thus, in order to reproduce the observed broadening of the eigenmodes, our ansatz for the imaginary part of the acoustic and optical mode eigenenergies reads as

$$\Delta E_{ac} = -i\chi_{11} \left(3 - \sum_n \cos k \cdot \boldsymbol{\alpha}_n \right)$$
$$- i\chi_{12} \left(3 - \sum_n \cos k \cdot \boldsymbol{\beta}_n \right), \quad (6)$$

$$\Delta E_{op} = -i\chi_2. \quad (7)$$

We extract the values of the parameters χ_{11}, χ_{12} and χ_2 by fitting Eqs. (6) and (7) to the *ab initio* results of

Ref. [44] (see Supplemental Material [48]). The band spectra and corresponding broadenings are shown in Fig. 1(b) for $\chi_{11} = 1.41$ meV, $\chi_{12} = -0.415$ meV, $\chi_2 = 3$ meV, $J = 1.2$ meV, $J_2 = 0.02J$, $S = 3/2$, $B = 0.04JS = 0.93$ T and $D = 0.8J/\sqrt{3}$. At the Γ point, the acoustic mode displays no broadening, in disagreement with ferromagnetic resonance measurements of common magnetic materials. This discrepancy most likely occurs because the analysis of Ref. [44] neglects magnon-magnon relaxation. However, we have verified that incorporating a constant dissipation term according to long-wavelength Landau-Lifshitz-Gilbert (LLG) phenomenology [49–52] does not affect qualitatively our results.

From Eqs. (4), (5), (6), and (7), the acoustic E_{ac} and optical E_{op} complex eigenenergies can be written as

$$E_{\text{ac(op)}} = h_0 \mp \sqrt{h_x^2 + h_y^2 + h_z^2} + \Delta E_{\text{ac(op)}}. \qquad (8)$$

The diagonal Hamiltonian $\mathcal{H}_d = \text{diag}(E_{\text{ac}}, E_{\text{op}})$ can be related to a non-Hermitian Hamiltonian $\mathcal{H}_{\text{nh}}$ in the basis of the lattice operators $a_{\boldsymbol{k}}$ and $b_{\boldsymbol{k}}$ via the unitary transformation $U\mathcal{H}_d U^{-1} = \mathcal{H}_{\text{nh}}$, where U is a matrix composed of the eigenvectors of $\mathcal{H}$, i.e., the optical and acoustic eigenmodes of the Hermitian honeycomb lattice (see Supplemental Material [48]). The Hamiltonian $\mathcal{H}_{\text{nh}}$ can be written explicitly as

$$\mathcal{H}_{\text{nh}} = \sum_{i=0,x,y,z} \sum_{\boldsymbol{k}} \Psi_{\boldsymbol{k}}^{\dagger} (\tilde{h}_i \sigma_i) \Psi_{\boldsymbol{k}}, \qquad (9)$$

where $\tilde{h}_0 = h_0 + B_0$ and $\tilde{h}_i = h_i(1 + A_0)$ for $i = x, y, z$, with

$$A_0 = \frac{\Delta E_{\text{op}} - \Delta E_{\text{ac}}}{2\sqrt{h_x^2 + h_y^2 + h_z^2}}, \quad B_0 = \frac{\Delta E_{\text{op}} + \Delta E_{\text{ac}}}{2}. \qquad (10)$$

An inverse Fourier transformation yields the real-space non-Hermitian Hamiltonian as (see Supplemental Material [48])

$$
\begin{aligned}
\mathcal{H}_{\text{nh}} = &\left[3JS + 6J_2S + B - \frac{i}{2}(\chi_2 + 3\chi_{11} + 3\chi_{12}) \right] \\
&\times \sum_i (a_i^{\dagger} a_i + b_i^{\dagger} b_i) \\
&+ \left(-J_2 S + \frac{i\chi_{12}}{4} \right) \sum_{\langle\langle i,j \rangle\rangle} (a_i^{\dagger} a_j + a_j^{\dagger} a_i + b_i^{\dagger} b_j + b_j^{\dagger} b_i) \\
&- JS \sum_{\langle i,j \rangle} \left[1 - \frac{i(\chi_2 - 3\chi_{11} - 2\chi_{12})}{2S\sqrt{3(J^2 + 2D^2)}} \right] (a_i^{\dagger} b_j + b_i^{\dagger} a_j) \\
&- DS \sum_{\langle\langle i,j \rangle\rangle} v_{ij} \left[i + \frac{\chi_2 - 3\chi_{11} - 2\chi_{12}}{2S\sqrt{3(J^2 + 2D^2)}} \right] \\
&\times (a_i^{\dagger} a_j - a_j^{\dagger} a_i + b_i^{\dagger} b_j - b_j^{\dagger} b_i) + ..., \qquad (11)
\end{aligned}
$$

where $+...$ indicates purely dissipative higher-order-nearest-neighbor terms. By setting $\chi_{11,12,2} = 0$ in Eq. (11), one can recover the Hermitian Hamiltonian (3). As shown by Eq. (11), the non-Hermitian terms take the form of on-site dissipation terms and of nonlocal dissipative couplings, which resemble the well-known dissipative nonlocal coupling terms due to electron-mediated spin pumping [53,54].

Here we retain only dissipative terms that have a nondissipative counterpart; however, accounting for purely dissipative higher-order-nearest-neighbor terms does not affect qualitatively our results (see Supplemental Material [48]).

Skin effect. To investigate the breakdown of the bulk-edge correspondence and the emergence of the magnetic skin effect, we diagonalize the Hamiltonian (11) numerically under the open boundary conditions (OBC). We consider a nanoribbon with zigzag and chair terminations along, respectively, the x and y direction. Figures 2(a) and 2(b) show the discrepancy between the open and periodic boundary condition (PBC) effective spectra [55], which is symptomatic of a breakdown of the bulk-edge correspondence. From the PBC effective spectra, it is easy to see that the complex acoustic (blue) and optical (orange) bands do not cross a reference line in the complex-energy plane: thus, the system has a line gap [56,57]. It is worth mentioning that, while in $1d$ systems the emergence of the skin effect is ascribed to a point-gap topology [10], this relation does not necessarily hold in higher-dimensional systems, in which a macroscopic accumulation of states at the boundary has been observed in the presence of a line gap as well [58].

Analogously to its Hermitian counterpart, the inversion-symmetry-breaking DM interactions break the time-reversal symmetry of the magnon Hamiltonian, yielding a $\mathbb{Z}$ topological order (i.e., both the Hermitian and non-Hermitian Hamiltonian belong to symmetry class A). Using Fukui's algorithm [59], we find $c_{\text{ac(opt)}}^{\text{nB}} = \pm 1$, where c^{nB} is non-Bloch Chern number introduced by Ref. [60]. The corresponding topological magnon edge states can be clearly visualized in the real-energy-gapped region of the OBC spectrum shown in Fig. 2(a).

As a measure of the localization of the bulk eigenstates at a boundary of the ribbon, we introduce the spatial distribution $|\psi(\boldsymbol{r})|^2$ of the density of the first N right eigenstates $\phi_n(\boldsymbol{r})$ of the OBC Hamiltonian (11), i.e., [43],

$$|\psi(\boldsymbol{r})|^2 = \frac{1}{N} \sum_{n=1}^{N} |\phi_n(\boldsymbol{r})|^2. \qquad (12)$$

Figure 2(c) displays the spatial distribution Eq. (12) of the eigenstates with energies up to $E = 0.247$ meV (corresponding to T ~ 2 K with $N = 79$) [61], which is delocalized throughout the bulk. At higher energies, i.e., $E = 2.655$ meV (T ~ 30 K with $N = 2771$), Fig. 2(d) shows that a macroscopic number of bulk eigenstates localizes at the corners and edges the ribbon. Thus, at high enough temperature (but below the magnetic ordering temperature T_c), the skin effect appears.

The observed temperature dependence can be understood via the relation between the skin effect and spectral shape of the PBC spectra [43]. In correspondence of arc or line (finite effective spectral area) in complex energy space, the mapping from momenta to energy is $2d$ to $1d$ ($2d$): for a wave impinging at the boundary there are infinite (finite) reflection channels, and an open boundary eigenstate can (can not) be described as superposition of Bloch waves, as discussed in details in Ref. [43]. The red- and green-dashed lines in Fig. 2(a) show the energies at which Figs. 2(c) and 2(d) are plotted, respectively. Up to T ~ 2 K (red line), the acoustic spectrum is (approximately) a line. Thus, the skin effect is
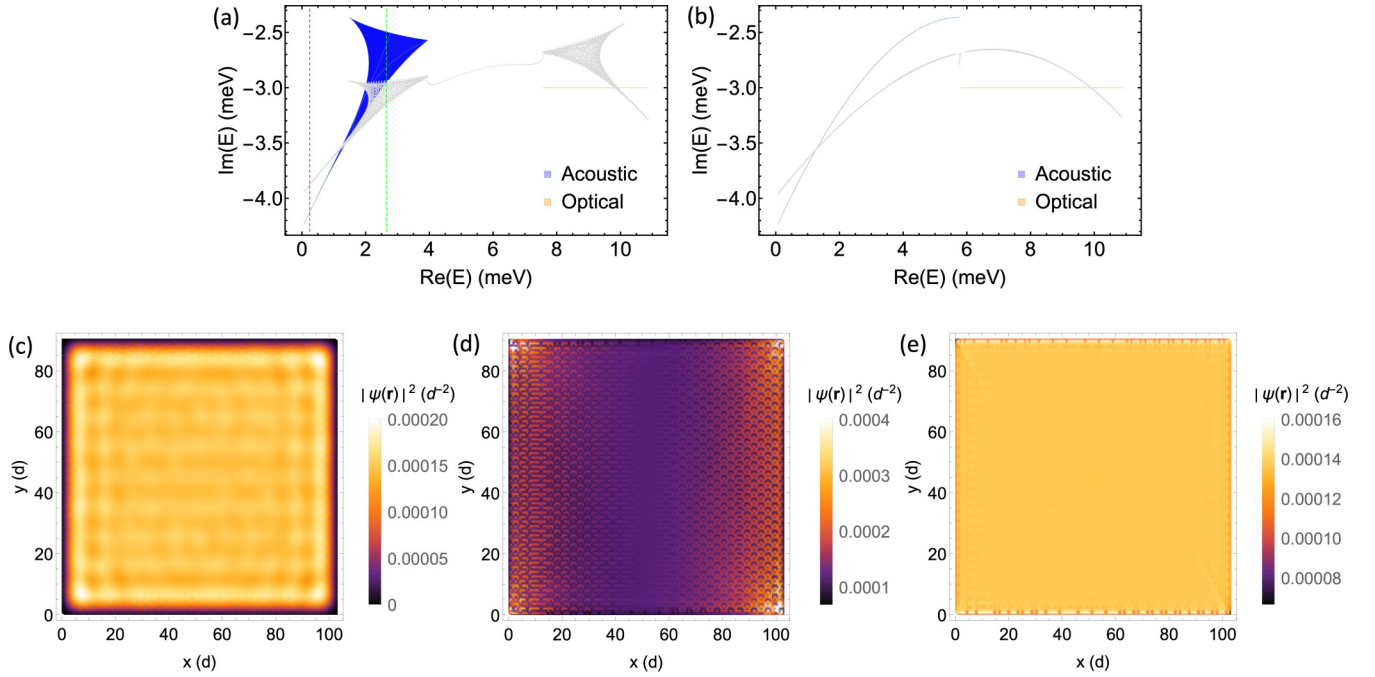
FIG. 2. [(a),(b)] PBC spectra of the acoustic (blue) and optical (orange) modes. The OBC eigenenergies of a nanoribbon with 60×60 lattice sites are shown in light-gray dots. (a) For $D = 0.8J/\sqrt{3}$. (b) For $D = 0$. [(c)–(e)] Spatial distribution of the density of the first N right eigenstates (12), (c) For $D = 0.8J/\sqrt{3}$ and $N = 79$, which corresponds to the energy $\mathrm{Re}E = 0.247$ meV. This energy is indicated by the dashed red line in Fig. 2(a), up to which the acoustic spectrum is (approximately) a line. The skin effect is absent. (d) For $D = 0.8J/\sqrt{3}$ and $N = 2771$, which corresponds to the energy $\mathrm{Re}E = 2.665$ meV. This energy is indicated by the dashed-green line in Fig. 2(a), around which the acoustic spectrum acquires a finite effective area. The skin effect appears. (e) For $D = 0$ and $N = 2771$ there is no skin effect as the acoustic spectrum reduces to the arc shown in Fig. 2(b).

not observable and bulk states behave as Bloch waves. This result is an agreement with the conventional long-wavelength LLG treatment of magnetic dissipation [51]. Instead, at higher energies (green line), the spectrum acquires a finite effective area and the skin effect appears.

In the absence of the DM interactions, the real and imaginary part of the energy are dependent, leading to the arc-like spectrum for both OBC and PBC displayed in Fig. 2(b). In agreement with the area law proposed by Ref. [43], the skin effect does not appear even at high temperatures, as shown in Fig. 2(e). Furthermore, in the absence of DMI, the Hamiltonian (4) becomes gapless and enters into a topologically trivial phase. The skin effect in Fig. 2(d) appears to be of the first-order type [43,62], i.e., a macroscopic number of modes localizes at arbitrary edges due to the non-Hermitian topological properties of the Hamiltonian. As shown by Fig. 2(d), the skin modes localized at left and right (armchair) edges, rather than at top and bottom (zigzag) terminations. This phenomenon can be understood by calculating the point-gap winding number [10,43] while setting periodic boundary conditions only along one direction, i.e., effectively reducing the dimensionality of the system to $1d$. We find that the point-gap winding number is vanishing for PBC along the y direction, while it is nonzero for PBC along x direction, which implies a localization of skin modes along the left and right edges, in agreement with Fig. 2(d) (also see Supplemental Material [48]).

The nonlocality of the magnon-phonon driven dissipation (6) plays also a key role. For $D \neq 0$ and $\chi_{12} = 0$, the skin ef-

fect does not appear even if the PBC spectrum of the acoustic eigenmode has a finite area. When $\chi_{12} = 0$, the $\boldsymbol{k}$-dependent term introducing nonlocal dissipation (6) reduces to

$$\Delta E_{\mathrm{ac}}^{\mathrm{nl}} = \chi_{11} \sum_n \cos \boldsymbol{k} \cdot \boldsymbol{\alpha}_n. \tag{13}$$

By including the nonlocal dissipation (13) in Eq. (4) and performing an inverse Fourier transformation, we find that the non-Hermitian contribution (13) vanishes in real space due to the symmetry of the honeycomb lattice (see Fig. S2 within the Supplemental Material [48]). Thus, the resulting real space Hamiltonian is equivalent to one derived by accounting only for the constant term $\propto -i\chi_{11}$ in Eq. (6), which yields a PBC spectrum with vanishing spectral area (i.e., a line). We have verified that in this scenario the skin effect does not appear even in the high frequency regime. This suggests that the area law proposed by Ref. [43] should be modified in order to take into account only terms that survive upon inverse Fourier transformation and lead to a spectral area that here we call "effective". The nonlocal contribution $\propto \chi_{12} \sum_n \cos \boldsymbol{k} \cdot \boldsymbol{\beta}_n$, instead, is not wiped out by lattice symmetry and, in conjunction with the DM interactions, yields the skin effect.

At a given temperature T [63], the skin effect is maximized by strong DM interactions, whose strength is proportional to the effective area of the PBC acoustic spectrum. A weak exchange coupling J leads to a reduced real-energy bandwidth of the acoustic magnon spectrum, which results in an amplified skin effect at a given frequency. The parameters χ_{11} and χ_2 lead to a featureless shift of the imaginary part

of the acoustic and optical eigenenergies, respectively, while χ_{12} contributes to the spectral area. Finally, it is worth to remark that the density of right eigenstates (12) plotted in Figs. 2(c)–2(e) might be naively interpreted as a magnon local density of states localized at an edge, which could be easily probed experimentally. However, the definition of the physical observables of non-Hermitian systems with broken bulk-edge correspondence, which are yet relatively unexplored in two and higher dimensions, require special care since they have to be defined on a biorthogonal basis and on the real-space lattice [2,14,64–66]. We will address this problem in future investigations.

Discussion and outlook. In this paper, we have explored the emergence of the skin effect in magnetic systems. We have proposed a phenomenological approach to derive non-Hermitian Hamiltonian terms that are allowed by the symmetries of the lattice model and reproduce the band broadening observed in experimental data. We have shown that, while adopting such phenomenological approach, the "area law" proposed by Ref. [43] should be replaced by the "effective area law" as a criteria for the emergence of the skin effect. Our phenomenological approach, combined with the "effective area law", can be easily applied to a wide class of

dissipative magnetic systems to identify a solid-state testbed of the skin effect that does not require *ad hoc* non-Hermitian engineering and whose properties can be controlled by tuning temperature and external magnetic fields.

As an example of our method, we have focused on a spin-orbit-coupled vdW magnet and we have found that the skin effect appears in at high enough temperatures when both nonlocal dissipative terms [67] and DM interactions are present. Furthermore, we have shown that the overall temperature trend of the skin effect can be understood through spectral shape of the PBC complex energy spectrum of the acoustic magnon mode. The interplay between DMI and the emergence of the skin effect should be further investigated. Future work should investigate the general physical properties that might yield the emergence of the skin effect in magnetic systems, explore experimental protocols to probe the localization of the bulk skin modes, and address the microscopic mechanisms underlying our phenomenological model.

[1] B. A. Bernevig, *Topological Insulators and Topological Superconductors* (Princeton University Press, Princeton, 2013).

[2] F. K. Kunst, E. Edvardsson, J. C. Budich, and E. J. Bergholtz, Phys. Rev. Lett. **121**, 026808 (2018).

[3] Z. Gong, Y. Ashida, K. Kawabata, K. Takasan, S. Higashikawa, and M. Ueda, Phys. Rev. X **8**, 031079 (2018).

[4] S. Yao and Z. Wang, Phys. Rev. Lett. **121**, 086803 (2018).

[5] K. Yokomizo and S. Murakami, Phys. Rev. Lett. **123**, 066404 (2019).

[6] C. H. Lee and R. Thomale, Phys. Rev. B **99**, 201103(R) (2019).

[7] F. Song, S. Yao, and Z. Wang, Phys. Rev. Lett. **123**, 170401 (2019).

[8] N. Okuma and M. Sato, Phys. Rev. Lett. **123**, 097701 (2019).

[9] D. S. Borgnia, A. J. Kruchkov, and R.-J. Slager, Phys. Rev. Lett. **124**, 056802 (2020).

[10] N. Okuma, K. Kawabata, K. Shiozaki, and M. Sato, Phys. Rev. Lett. **124**, 086801 (2020).

[11] Z. Yang, K. Zhang, C. Fang, and J. Hu, Phys. Rev. Lett. **125**, 226402 (2020).

[12] C. H. Lee, L. Li, R. Thomale, and J. Gong, Phys. Rev. B **102**, 085151 (2020).

[13] C. H. Lee and S. Longhi, Commun. Phys. **3**, 1 (2020).

[14] Y. Yi and Z. Yang, Phys. Rev. Lett. **125**, 186802 (2020).

[15] L. Jin and Z. Song, Phys. Rev. B **99**, 081103(R) (2019).

[16] S. Longhi, Phys. Rev. Research **1**, 023013 (2019).

[17] X. Zhu, H. Wang, S. K. Gupta, H. Zhang, B. Xie, M. Lu, and Y. Chen, Phys. Rev. Research **2**, 013280 (2020).

[18] K. Xu, X. Zhang, K. Luo, R. Yu, D. Li, and H. Zhang, Phys. Rev. B **103**, 125411 (2021).

[19] L.-J. Lang, Y. Weng, Y. Zhang, E. Cheng, Q. Liang, Phys. Rev. B **103**, 014302 (2021).

[20] T. Hofmann, T. Helbig, F. Schindler, N. Salgo, M. Brzezińska, M. Greiter, T. Kiessling, D. Wolf, A. Vollhardt, A. Kabaši, C. H. Lee, A. Bilušić, R. Thomale, and T. Neupert, Phys. Rev. Research **2**, 023265 (2020).

[21] T. Helbig, T. Hofmann, S. Imhof, M. Abdelghany, T. Kiessling, L. Molenkamp, C. Lee, A. Szameit, M. Greiter, and R. Thomale, Nat. Phys. **16**, 747 (2020).

[22] L. Xiao, X. Zhan, Z. Bian, K. Wang, X. Zhang, X. Wang, J. Li, K. Mochizuki, D. Kim, N. Kawakami *et al.*, Nat. Phys. **13**, 1117 (2017).

[23] S. Weidemann, M. Kremer, T. Helbig, T. Hofmann, A. Stegmaier, M. Greiter, R. Thomale, and A. Szameit, Science **368**, 311 (2020).

[24] A. Ghatak, M. Brandenbourger, J. van Wezel, and C. Coulais, Proc. Natl. Acad. Sci. USA **117**, 29561 (2020).

[25] P. A. McClarty and J. G. Rau, Phys. Rev. B **100**, 100405(R) (2019).

[26] A. Galda and V. M. Vinokur, Phys. Rev. B **94**, 020408(R) (2016).

[27] A. Galda and V. M. Vinokur, Sci. Rep. **9**, 17484 (2019).

[28] Y. Tserkovnyak, Phys. Rev. Research **2**, 013031 (2020).

[29] T. Jeffrey, W. Zhang, and J. Sklenar, Appl. Phys. Lett. **118**, 202401 (2021).

[30] H. Liu, D. Sun, C. Zhang, M. Groesbeck, R. Mclaughlin, and Z. V. Vardeny, Sci. Adv. **5**, eaax9144 (2019).

[31] B. Flebus, R. A. Duine, and H. M. Hurst, Phys. Rev. B **102**, 180408(R) (2020).

[32] J. Zhao, Y. Liu, L. Wu, C.-K. Duan, Y.-x. Liu, and J. Du, Phys. Rev. Applied **13**, 014053 (2020).

[33] X. Zhang, K. Ding, X. Zhou, J. Xu, and D. Jin, Phys. Rev. Lett. **123**, 237202 (2019).

[34] T. Yu, Y.-X. Zhang, S. Sharma, X. Zhang, Y. M. Blanter, and G. E. W. Bauer, Phys. Rev. Lett. **124**, 107202 (2020).

[35] S. Streib, N. Vidal-Silva, K. Shen, and G. E. W. Bauer, Phys. Rev. B **99**, 184442 (2019).

[36] E. Balcar, Le J. phys., Colloq. **32**, C1-701 (1971).

[37] X. Wu, Z. Liu, and T. Luo, J. Appl. Phys. **123**, 085109 (2018).

[38] S. M. Rezende and R. M. White, Phys. Rev. B **18**, 2346 (1978).

[39] L. Berger, J. Phys. Chem. Solids **38**, 1321 (1977).

[40] E. D. Thompson, J. Appl. Phys. **36**, 1133 (1965).

[41] R. B. Woolsey and R. M. White, Phys. Rev. **188**, 813 (1969).

[42] D. L. Huber, *B. Spin wave lifetimes in YIG Datasheet from Landolt-Börnstein - Group III Condensed Matter*, Part of in SpringerMaterials Volume 4A, edited by K.-H. Hellwege and A. M. Hellwege (Springer-Verlag, Berlin, Heidelberg, 1970).

[43] K. Zhang, Z. Yang, and C. Fang, Nat. Commun. **13**, 2496 (2022).

[44] K. Wang, X. Xu, Y. Cheng, M. Zhang, J.-S. Wang, H. Wang, and G. Zhang, Appl. Phys. Lett. **118**, 023102 (2021).

[45] K. Wang, J. He, M. Zhang, H. Wang, and G. Zhang, Nanotechnology **31**, 435705 (2020).

[46] Y. Liu, L.-S. Xie, Z. Yuan, and K. Xia, Phys. Rev. B **96**, 174416 (2017).

[47] It breaks the translational symmetry because the relaxation in momentum space should also be periodic due to the periodicity of the Brillouin zone (BZ). For k^2, the relaxation would increase to extremely large values when k is large, which is unphysical.

[48] See Supplemental Material at http://link.aps.org/supplemental/10.1103/PhysRevB.105.L180406 for (i) more details on the fitting; (ii) details on this derivation; and (iii) details on the inverse Fourier transformation.

[49] T. L. Gilbert, Phys. Rev **100**, 1243 (1955).

[50] E. Lifshitz and L. Pitaevskii, *Statistical Physics: Theory of the Condensed State*, Course of Theoretical Physics No. v. 9 (Elsevier Science, Amsterdam, 2013).

[51] T. L. Gilbert, IEEE Trans. Magn. **40**, 3443 (2004).

[52] M. C. Hickey and J. S. Moodera, Phys. Rev. Lett. **102**, 137601 (2009).

[53] B. Heinrich, Y. Tserkovnyak, G. Woltersdorf, A. Brataas, R. Urban, and G. E. Bauer, Phys. Rev. Lett. **90**, 187601 (2003).

[54] Y. Tserkovnyak, A. Brataas, and G. E. Bauer, Phys. Rev. B **67**, 140404 (2003).

[55] The effective spectral area is obtained by neglecting the contribution proportional $\propto -\chi_{11} \sum_j \cos \boldsymbol{k} \cdot \boldsymbol{\alpha}_j$ in Eq. (6). More details on the effective area law we propose are discussed in the following main text and in the Supplemental Material [48].

[56] H. Shen, B. Zhen, and L. Fu, Phys. Rev. Lett. **120**, 146402 (2018).

[57] K. Kawabata, K. Shiozaki, M. Ueda, and M. Sato, Phys. Rev. X **9**, 041015 (2019).

[58] C. H. Lee, L. Li, and J. Gong, Phys. Rev. Lett. **123**, 016805 (2019).

[59] T. Fukui, Y. Hatsugai, and H. Suzuki, J. Phys. Soc. Jpn. **74**, 1674 (2005).

[60] S. Yao, F. Song, and Z. Wang, Phys. Rev. Lett. **121**, 136802 (2018).

[61] Here we include equally-weighed contributions of magnon states up to a given energy.

[62] K. Kawabata, M. Sato, and K. Shiozaki, Phys. Rev. B **102**, 205118 (2020).

[63] Here we consider temperatures below the magnetic ordering temperature T_c, usually ~50 K for vdW magnets.

[64] D. C. Brody, J. Phys. A: Math. Theor. **47**, 035305 (2013).

[65] T. Curtright and L. Mezincescu, J. Math. Phys. **48**, 092106 (2007).

[66] L. N. Chang, Z. Lewis, D. Minic, and T. Takeuchi, J. Phys. A: Math. Theor. **46**, 485306 (2013).

[67] We note that magnon-magnon interaction can lead as well to a $k-$dependent term to the dissipation, which could also be added to our ansatz in a similar fashion and might lead to a stronger skin effect.